Solid State Phenomena
ISSN: 1662-9779, Vol. 388, pp 47-55
doi:10.4028/p-Ew8Pjl

Submitted: 2025-12-21
Revised: 2026-02-23
Accepted: 2026-02-23
Online: 2026-04-15

The Interaction of N- and R-Values and Total Elongation in Forming Limit Curves' Theories

Borbely Richard[1,3,a], Toth-Nagy Bendeguz V.[1,b], Kecskes Bertalan[2,c], Keresztes Robert Zs.[3,d], Beres Gabor J.[1,e*]

[1]Innovative Vehicles and Materials Department, John von Neumann University, Hungary

[2]HILTI Tool Ltd., Kecskemét Factory, Hungary

[3]Doctoral School of Technical Sciences, Hungarian University of Agriculture and Life Sciences, Hungary

[a]borbely.richard@nje.hu, [b]toth-nagy.bendeguz@nje.hu, [c]Bertalan.Kecskes@hilti.com
[d]keresztes.robert.zsolt@uni-mate.hu, [e*]beres.gabor@nje.hu

Keywords: forming limit curves, theoretical calculations, tensile test.

Abstract. Forming limit curve (FLC) is the most commonly used failure criterion in the sheet metal forming industry. All commercial simulation software uses this concept to evaluate failure strains and to detect the most critical section(s) of the workpiece. The laboratory determination of the FLC is standardized. However, because experimental measurement is cumbersome, theoretical calculations of FLCs using mechanical properties from well-defined test conditions are of great interest. Several such approaches have been proposed in the literature. This paper presents calculated FLCs using the models of Abspoel et al., Stören and Rice and Swift. All the equations include tensile tests data that have been measured physically at room temperature, with quasi-static strain rates. Calculated results of DC04 cold rolled steel sheet with relatively high plastic anisotropy coefficient was compared to a nearly isotropic DP800 high strength steel. Based on the results it is observed that r-value influences the shape of the left-hand side of the FLC as well as the plane strain point significantly, for the DC04 sheet. These effects are less pronounced for the DP800 material, which has lower r-value. At the same time, n-value and total elongation raise or lower the curves, generally. These observations are briefly explained by function analyses using fictitious r-values in the calculations.

Introduction

Theoretical prediction of sheet failure through Forming Limit Curves (FLCs) has long been a central topic in sheet metal forming research. Literature fundamentally distinguishes analytical equations obtained by either simplified constitutive models, statistical, or semi-empirical approaches. In addition to this, more sophisticated numerical descriptions are also available. However, the more realistic modeling of strain hardening leads to advanced solutions, many finite element (FE) software still use analytical FLC equations as input parameters to assign failure criterion to the applied sheet material. These types of equations often contain mechanical properties from well-defined tests, such as tensile tests. Although evaluating the entire formability from results of only uni-axial stress state is a necessary simplification, the application of these equations is still widespread in the industrial practice, according to the authors' experiences.

Naturally, there is a lot of valuable literature that should be referenced in this topic, but here, in this introduction, literature [1] deserves special attention first, as it contains a logical overview of the FLC theories. Accordingly, the theoretical FLC models are broadly divided into the following groups:

- assuming homogeneous sheet:
  - necking theories,
  - bifurcation theories,
  - linearized theory of perturbations,
- assuming non-homogeneous sheet,
- semi-empirical theories.

The models developed by Hill [2], Swift [3] and Hora et al. [4] belong to the group of necking theories of homogenous sheets. Hill described the zero-extension phenomenon for the left-hand side of the FLC, which was extended by Swift with the maximum force theory. It is worth noting here that the Swift model is related to diffuse necking phenomenon instead of localized necking, but it still appears frequently in the relevant literature. Later, Hora et al. developed the modified maximum force criterion (known as MMFC), based on Swift's work.

The bifurcation theory belongs to the study of Stören and Rice [5], who assumed that the development of localized neck formation is inherent with the formation of a vertex on the yield surface. They used deformation theory to derivate the equation of the critical major strain, in which the most important parameter is the strain hardening exponent. In case of localized failure initiation developing from a surface defect, thus assuming non-homogeneous sheet, the most famous model is the Marciniak-Kuczynski theory [6]. In the field of semi-empirical models, authors highlight here the work of Abspoel et al. [7], Kumar [8], Keeler-Brazier [9] and Levy-Tyne [10]. Naturally, this is not a complete list of FLC calculation formulas, readers can find more information in recent review papers [11, 12, 13, 14].

This study deals with the presentation of tensile tests results and calculated FLCs for two steel sheets. For the investigation of different limit theories, approaches were selected from the group of necking (Swift), bifurcation (Stören-Rice) and semi-empirical (Abspoel et al.) models. Thereafter, function analyses were carried out to present comparisons, with the aim of helping the practical work of FE software users. The applied materials to which the calculation have been performed were DC04 and DP800 steel sheets. The necessary physical data have been obtained from tensile tests in every 15° to the rolling direction. Comparisons and explanations of the FLC-s are presented in the rest of the paper.

Materials and Methods

Applied materials.

Commercial, cold rolled DC04 steel sheet and DP800 high strength steel sheet were tested in this research. The nominal sheet thickness was 1 mm, for each material. Representative micrographs are shown by Fig. 1, illustrating the grain morphology and the ferrite-martensite volume fraction for the DP steel. The mechanical properties were obtained by standard tensile tests, which will be discussed in the next subchapter.

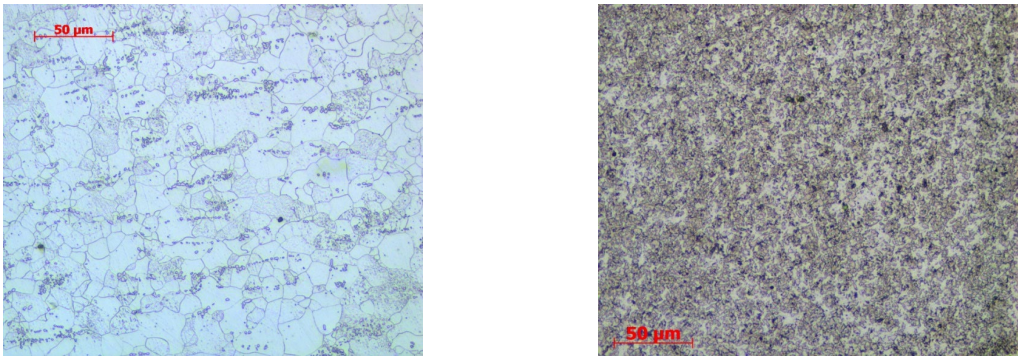

Fig. 1. Microstructure of DC04 (left) and DP800 (right).

Measurement method: tensile tests.

Standard uniaxial tensile tests (ISO 6892-1) were performed at room temperature on A_{80} specimens, where footnote 80 refers to the initial gauge length. The specimen orientations were 0°, 15°, 30°, 45°, 60°, 75°, and 90° with respect to the rolling direction. The tests were carried out on an Instron 5900R 4482 universal testing equipment with constant crosshead speed of 4 mm/min. It led to less than $1 \cdot 10^{-3}$ s^{-1} initial strain rate. The strain measurements were supported by an Instron AVE 5585 video extensometer. The measurement arrangement as well as real and schematic specimens are depicted on Fig. 2.

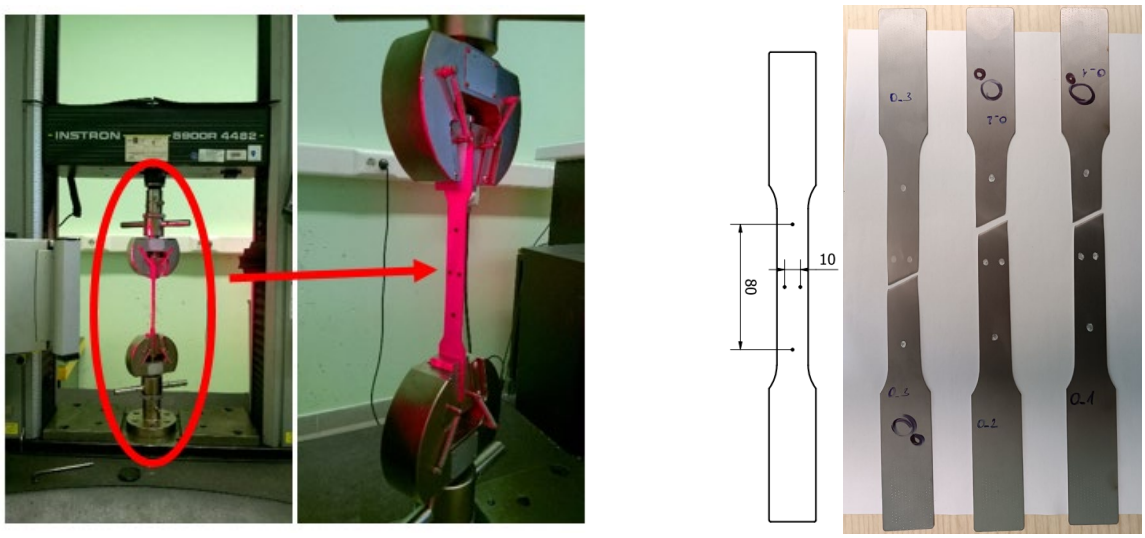

Fig. 2. Tensile test equipment and specimens (dimensions are in mm).

Engineering stress-stain, true plastic stress-strain and r-value evolution diagrams were extracted from the raw data, for both materials. Fig 3 shows the results parallel to the rolling direction. Strain hardening exponent (n-value), coefficient of plastic anisotropy (r-value) and total elongation (A_{80}) have received the most attention during the evaluation of the tensile tests. These parameters are main factors of the selected models, therefore their average values are listed directly next to the FLCs, in the later figures: Fig, 4, 5 and 7. The n-values were approximated based on the power law description (Eq. 1) [15].

$$\bar{\sigma} = K \cdot \bar{\varepsilon}^{n} , \quad (1)$$

in which K is strength coefficient.

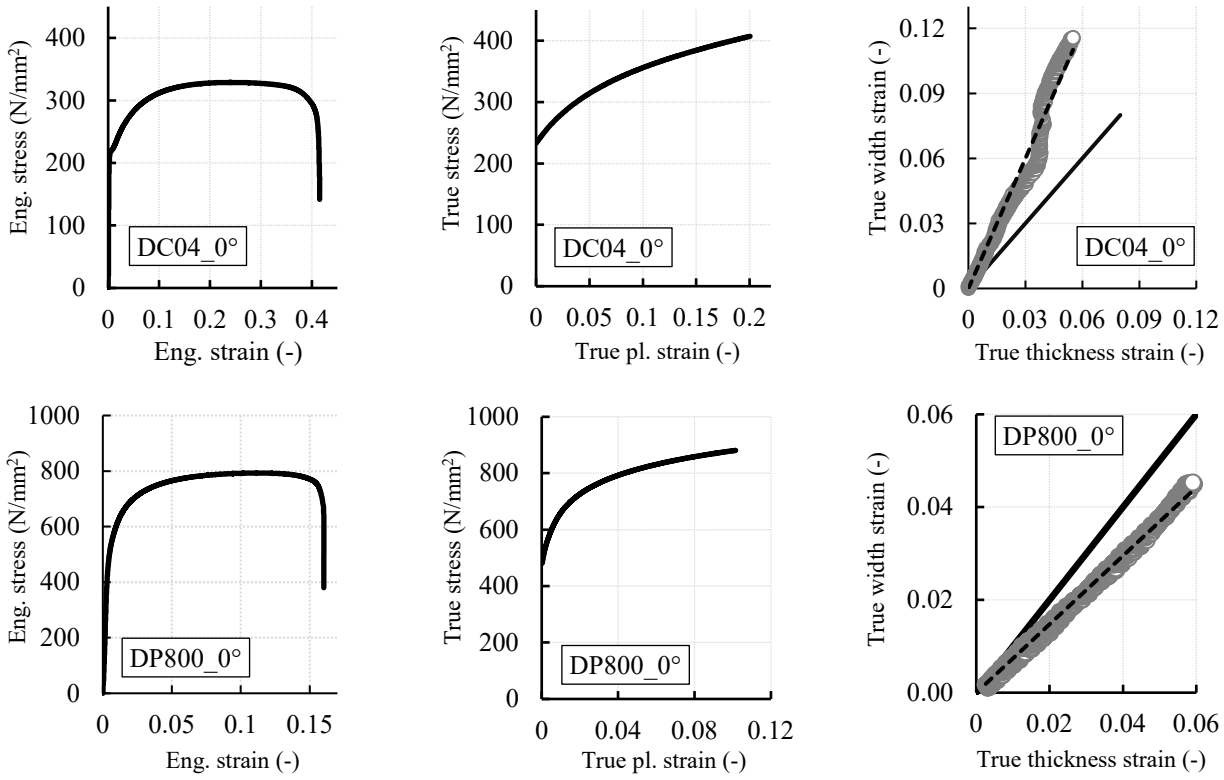

Fig. 3. Engineering (left) and true plastic (middle) stress-strain curves and the r-value's evolution (right) for DC04 and DP800 steel sheets.

FLC calculations from tension test data

The equations of Stören-Rice model [5] (considering n-value), Swift model [3] (considering n- and r-values), and the approach of Abspoel et al. [7] (considering r- and A_{80} values) are investigated in this chapter.

Stören-Rice equation.

This formula is derived from the assumption of a vertex development on the yield surface, at localized necking. Using the deformation theory with isotropic yield criterion, this research leads to the next two equations regarding critical (failure) major (ε_1^*) and (ε_2^*) minor strains:

$$\varepsilon_1^* = \frac{3\beta^2+n(2+\beta)^2}{2\cdot(2+\beta)\cdot(1+\beta+\beta^2)}\ , \tag{2}$$

$$\beta\varepsilon_1^* = \varepsilon_2^*;\ (-1 \le \beta \le 1)\ . \tag{3}$$

Substituting the measured n-values in seven orientations of both materials to Eq. 2, the calculated FLCs are shown in Fig. 4. The average n-values are also depicted on the left of Fig. 4, in descending order. It can be stated that the order of the FLCs follows the order of the n-values, because this is the only one varying material parameter. However, the distance between the curves is not consistently the same in all stress (strain) states. This observation applies for both materials, which is better traceable on the enlarged pictures on the right of Fig. 4.

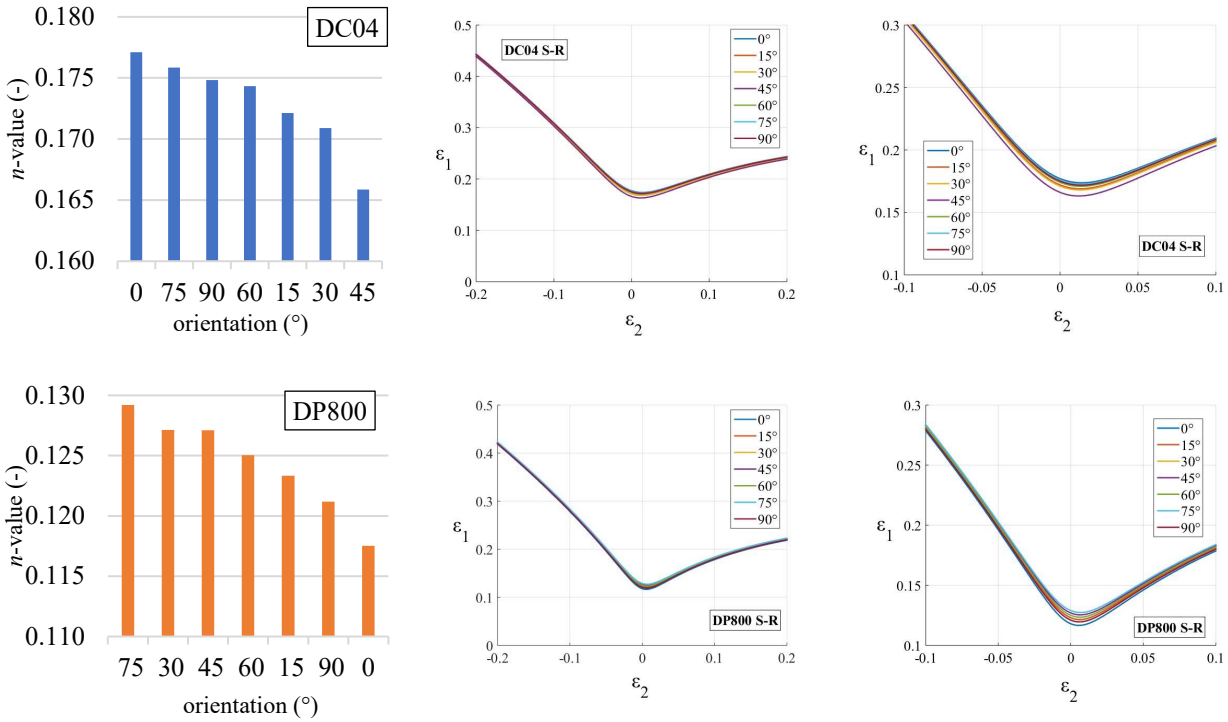

Fig. 4. N-values of different orientations in descending order (left), as well as calculated FLCs in the middle, supplemented with enlarged pictures on the right; DC04 above and DP800 below.

For understanding the underlying reason, function analysis was conducted by substituting in β the values taken in noteworthy strain states: plane strain (β = 0), equi-biaxial tension (β = 1) and uni-axial tension (β = -1/2). Eq. 4-6 display the result of the derivation:

$$\text{if } \beta = 0 \rightarrow \varepsilon_1^* = n\ , \tag{4}$$

$$\text{if } \beta = 1 \rightarrow \varepsilon_1^* = \frac{n+\frac{1}{3}}{2} = \frac{1}{2}n + \frac{1}{6}\ , \tag{5}$$

$$\text{if } \beta = -\frac{1}{2} \rightarrow \varepsilon_1^* = \frac{9n+3}{9} = n + \frac{1}{3}\ . \tag{6}$$

Based on this investigation, the critical major strains are equivalent with n-values in the plane strain state, causing the positions of the FLCs to be proportional to this parameter. Nevertheless, constants are dominant in equi-biaxial and uni-axial strain states, resulting in the curves converge closer to each other.

Swift equation.

The model originates from the assumption of maximum force criterion, $d\sigma_1 = \sigma_1 d\varepsilon_1$ and $d\sigma_2 = \sigma_2 d\varepsilon_2$. The limit strains' equations (Eq. 7 and 8) as well as the results of derivations (Eq. 9 and 10) can be found in [1], for the case of Hill'48 yield criterion [16].

$$\varepsilon_1^* = \frac{\sigma_1 \cdot \left(\frac{\partial f}{\partial \sigma_1}\right)^2 + \sigma_2 \cdot \left(\frac{\partial f}{\partial \sigma_2}\right) \cdot \left(\frac{\partial f}{\partial \sigma_1}\right)}{\sigma_1 \cdot \left(\frac{\partial f}{\partial \sigma_1}\right)^2 + \sigma_2 \cdot \left(\frac{\partial f}{\partial \sigma_2}\right)^2} \cdot n\,, \tag{7}$$

$$\varepsilon_2^* = \frac{\sigma_2 \cdot \left(\frac{\partial f}{\partial \sigma_1}\right)^2 + \sigma_1 \cdot \left(\frac{\partial f}{\partial \sigma_1}\right) \cdot \left(\frac{\partial f}{\partial \sigma_2}\right)}{\sigma_1 \cdot \left(\frac{\partial f}{\partial \sigma_1}\right)^2 + \sigma_2 \cdot \left(\frac{\partial f}{\partial \sigma_2}\right)^2} \cdot n\,. \tag{8}$$

$$\varepsilon_1^* = \frac{[1+r(1-\alpha)] \cdot \left(1 - \frac{2r}{1+r}\alpha + \alpha^2\right)}{(1+r)(1+\alpha) \cdot \left[1 - \frac{1+4r+2r^2}{(1+r)^2}\alpha + \alpha^2\right]} \cdot n\,, \tag{9}$$

$$\varepsilon_2^* = \frac{[(1+r)\alpha - r] \cdot \left(1 - \frac{2r}{1+r}\alpha + \alpha^2\right)}{(1+r)(1+\alpha) \cdot \left[1 - \frac{1+4r+2r^2}{(1+r)^2}\alpha + \alpha^2\right]} \cdot n\,. \tag{10}$$

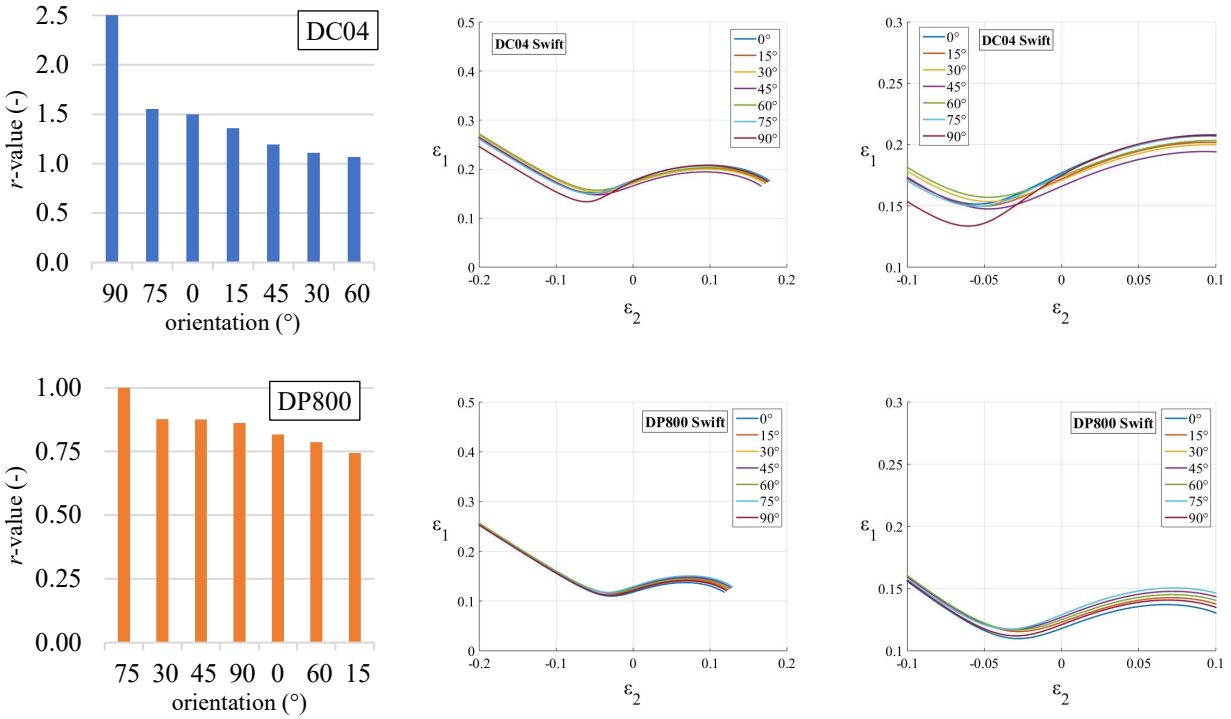

Fig. 5. R-values of different orientations in descending order (left), as well as calculated FLCs in the middle, supplemented with enlarged pictures on the right; DC04 above and DP800 below.

Although the enlarged images at the right of Fig. 5 highlight the order of the FLCs, the determination of whether the r- or n-value has stronger effect on the curves' position and shape, is doubtful. DP800 has the highest r-value in 75° to the rolling direction (followed by the specimens of 30° and 45°), which is the same for the n-value, too (Fig. 4). Still for this material, the curve located at the bottom belongs to the 0°orientation, which has the lowest n-, but the third from the bottom r-value. For the DC04 sheet, specimen 90° to the rolling direction has the highest r-value and gives the FLC located at the bottom, in plane strain tension. Even if, n-value is relatively high in this

orientation. In addition to this, it is also observed that average highest n-value (0° in Fig. 4) is unable to produce the highest curve position, in the same stress state. However, in equi-biaxial tension, the position of the curves is reordered again, presumably according to the extent of n-value (0° at the top, 45° at the bottom). It leads to the assumption that r- and n-values create a cross-effect in this model under certain stress states, which is not necessarily true for both materials.

For possible explanations, mathematical analyses have been performed by solving Eq. 9 and 10 for noteworthy stress states: $\alpha = 0$, $\alpha = 1/2$, $\alpha = 1$. Then critical major and minor strains were expressed for fictitious r-values (Fig. 6), next to taking n-value as constant 0.17.

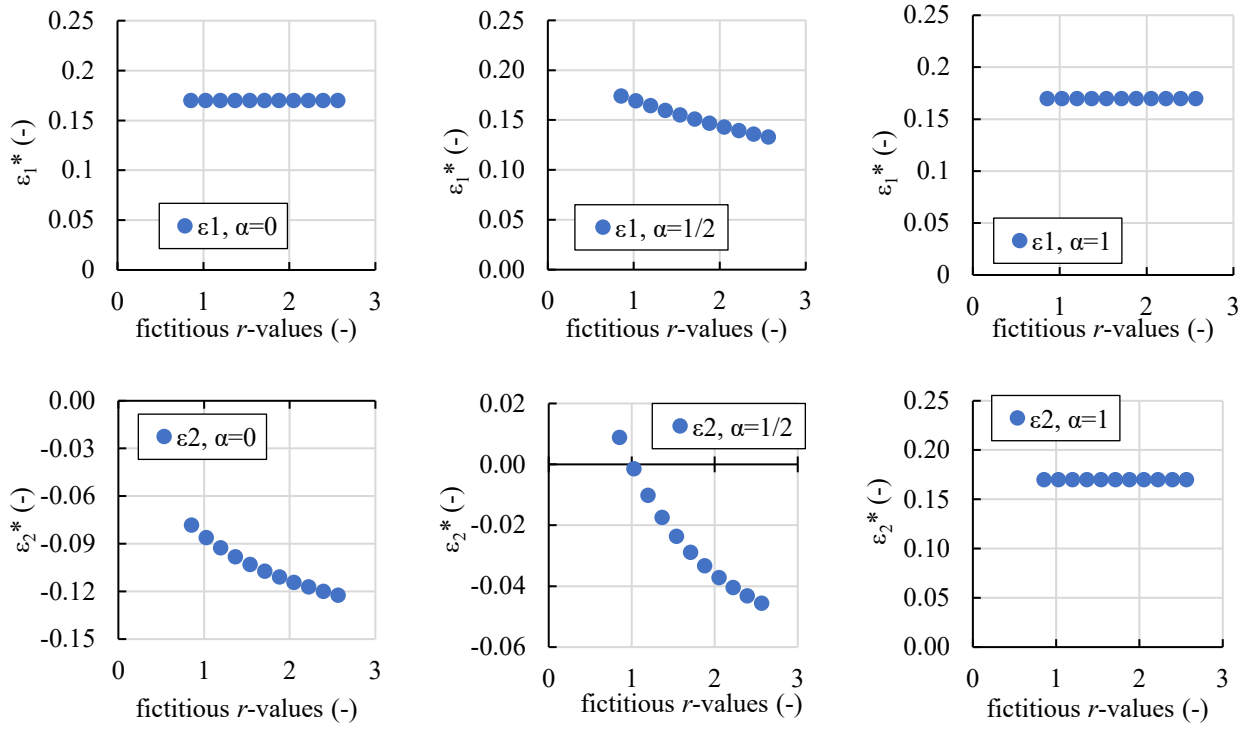

Fig. 6. Evolution of critical major strain in the function of r-value.

Fig. 6 shows that critical major strain is independent from the r-value in this current form of Swift model, in uni-axial and equi-biaxial tension loading. Besides, in plane strain tension, materials with higher r-value lead to lower critical major strain. The minor strain is always decreasing with increasing r-value, except in equi-biaxial stress state, causing the curves' shift to down and left.

Abspoel et al. equation.

This concept uses regression approximation to evaluate the limit strains from tensile tests results. Here, n-value does not get emphasis, but total elongation (A_{80}) dominates the outcome in all stress states. Plastic anisotropy coefficient comes to play only in the negative quadrant of the FLCs. Another difference is that the deformation is determined by some specific points of noteworthy stress states, instead of continuous function of limit strains. The equations for uni-axial tension, plane strain tension and equi-biaxial tension load cases are given by Eq. 11-14, considering the fact that the nominal sheet thickness is equal to unity.

Uni-axial stress state:

$$\varepsilon_1^* = (1 + 0.797 \cdot r^{0.701}) \cdot \frac{0.0626 \cdot A_{80}^{0.567}}{\sqrt{[1+(0.797 \cdot r^{0.701})^2]}}, \tag{11}$$

$$\varepsilon_2^* = -(0.797 \cdot r^{0.701}) \cdot \frac{0.0626 \cdot A_{80}^{0.567}}{\sqrt{[(1+(0.797 \cdot r^{0.701})^2]}}. \tag{12}$$

Plane strain stress state:

$$E_1^* = 0{,}0084 \cdot A_{80}\,. \tag{13}$$

Equi-biaxial stress state:

$$E_1^* = \varepsilon_2^* = 0{,}00215 \cdot A_{80} + 0{,}25 + 0{,}00285 \cdot A_{80}\,. \qquad (14)$$

Values of A_{80} of both materials in descending order as well as calculated FLCs are depicted by Fig. 7. The difference between the limit curves is highlighted by the enlarged pictures on the right side. Eq. 13 and 14 are linear functions of total elongation, and thus the FLCs' order is clearly defined by the total elongation in plane strain tension and equi-biaxial tension stress states. Plastic anisotropy distorts only the left-hand side of the limit curves, with the combined effect of the total elongation.

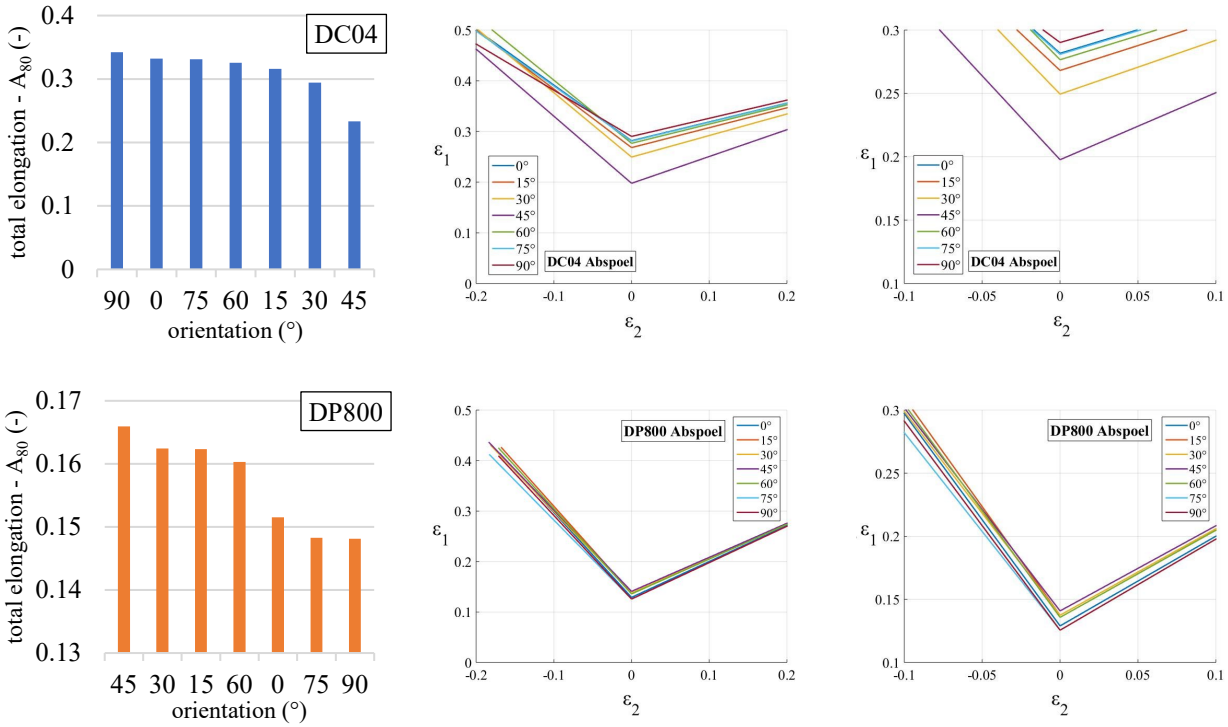

Fig. 7. Total elongations of different orientations in descending order (left), as well as calculated FLCs in the middle, supplemented with enlarged pictures on the right; DC04 above and DP800 below.

Assuming a constant for A_{80} and substituting fictitious r-values into Eq. 11-12, the evolution of the critical major and minor strains in the function of the r-value can be monitored for uni-axial stress state, in Fig. 8. This figure shows that A_{80} proportionally increases both ε_1^* and ε_2^*, and the effect of the r-value is stronger on the critical minor strain (ε_2^*). It means that r-value tilts the FLC to the left, in this model. In terms of critical major strain (ε_1^*), which is almost independent from plastic anisotropy coefficient, it still is worth noting that it has local maximum at $r \approx 1.4$ according to this formula.

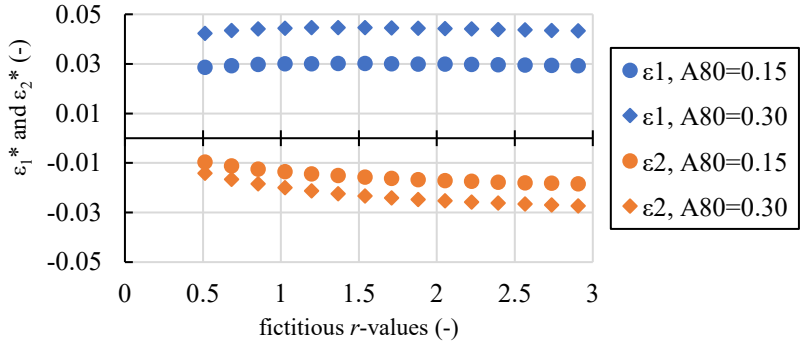

Fig. 8. Evolution of critical major and minor strains in the function of fictitious r-values, in uni-axial stress state.

Summary

The current paper discusses three different calculation methods of FLC evaluation, for which the necessary experimental data is obtained from tensile tests. The applied formulas are arbitrary selected from the literature, but they belong to different logical groups of theories. Tensile tests of DC04 and DP800 steels in room temperature were performed in seven orientations, from 0° to 90° to the rolling direction. FLCs were then calculated separately in each direction, and the observed trends were compared and described for the two materials in this study.

Based on the current observations, the higher the n-value and the total elongation, the higher is position of the FLCs, in general. Besides, the role of the r-value is slightly more complicated. The increase of plastic anisotropy coefficient caused the shift to down and left of the plane strain point in the Swift equation, for the DC04 sheet. Similar effects for the DP800 material are not observed. In the model of Abspoel et al., the plane strain point is independent from the r-value, but the FLCs are tilted to the left in the negative quadrant. This phenomenon also appears more prominently for the DC04 sheet. Therefore, the precise determination of the r-value is more important in terms of the shape of the FLC in the negative quadrant as well as the position of the calculated plane strain point. Nevertheless, both these modeled behaviors are more significant for steels with higher r-value.

Acknowledgement

We acknowledge the professional support of the Ministry of Culture and Innovation's New National Excellence Program (grant code EKÖP-2024-00020), financed by the National Research, Development and Innovation Fund in Hungary.
The research was carried out in connection with the project entitled „Development of new innovative chisel generations" 2020-1.1.2-PIACI-KFI-2020-00148 financed by National Research, Development and Innovation Fund in Hungary.

References

[1] D. Banabic, "Sheet Metal Forming Pocesses, Constitutive Modeling and Numerical Simulation", Springer-Verlag Berlin Heidelberg, 2010, doi: 10.1007/978-3-540-88113-1.

[2] R. Hill, "On discontinuous plastic states, with special reference to localized necking in thin sheets", Journal of the Mechanics and Physics of Solids, vol 1. pp. 19-30, 1952.

[3] H. W. Swift, "Plastic instability under plane stress", Journal of the Mechanics and Physics of Solids, vol. 1. pp. 1-18, 1952.

[4] P. Hora, L. Tong, and B. Berisha, "Modified maximum force criterion, a model for the theoretical prediction of forming limit curves," International Journal of Material Forming, vol. 6, pp. 267–279, 2013, doi: 10.1007/S12289-011-1084-1.

[5] S. Stören and J. R. Rice, "Localized necking in thin sheets," J Mech Phys Solids, vol. 23, pp. 421–441, 1975, doi: 10.1016/0022-5096(75)90004-6.

[6] Z. Marciniak, K. Kuczynski, "Limit strains in the processes of stretch-forming sheet metal", Int. J. Mech. Sci. vol. 9, pp. 609-620, 1967.

[7] M. Abspoel, M. E. Scholting, and J. M. M. Droog, "A new method for predicting Forming Limit Curves from mechanical properties," J Mater Process Technol, vol. 213, pp. 759–769, 2013, doi: 10.1016/J.JMATPROTEC.2012.11.022.

[8] S. K. Paul, "Prediction of complete forming limit diagram from tensile properties of various steel sheets by a nonlinear regression based approach," J Manuf Process, vol. 23, pp. 192–200, 2016, doi: 10.1016/j.jmapro.2016.06.005.

[9] T. Altan, A.E. Tekkaya, Sheet Metal Forming – Fundamentals, ASM International, 2012.

[10] B.S. Levy, C.J. Van Tyne, “Determination of a Stress-Based Forming Limit Curve from Mechanical Properties,” IDDRG Conference Proc., Shanghai, China, 2015.

[11] D. Banabic, F. Barlat, O. Cazacu, T. Kuwabara, “Advances in anisotropy and formability”, International Journal of Material Forming, 3:165-189, 2010, doi: 10.1007/s12289-010-0992-9.

[12] D. Banabic, F. Barlat, O. Cazacu, T. Kuwabara, “Advances in anisotropy of plastic behaviour and formability of sheet metals”, International Journal of Material Forming, 2020, doi: 10.1007/s12289-020-01580-x.

[13] S. Bruschi et al., “Testing and modeling of material behaviour and formability in sheet metal forming”, CIRP Annals – Manufacturing Technology, 63, pp. 727-749, 2014, doi: 10.1016/j.cirp.2014.05.005.

[14] Sz. Szalai, D. Harangozó, I. Czinege, “Az alakíthatósági határgörbe meghatározása és modellezése”, Anyagvizsgálók Lapja, II. pp. 39-52, 2021.

[15] Á. Nádai, A. M. Wahl, and E. C. Bingham, “Plasticity, A Mechanics of the Plastic State of Matter,” J Rheol (N Y N Y), vol. 2, pp. 455–456, 1931, doi: 10.1122/1.2116408.

[16] R. Hill, “A theory of the yielding and plastic flow of anisotropic metals,” Proc R Soc Lond A Math Phys Sci, vol. 193, pp. 281–297, 1947, doi: 10.1098/RSPA.1948.0045.